MADRID
inter.noise 2019
June 16 - 19
NOISE CONTROL FOR A BETTER ENVIRONMENT

Configurations of ring-shaped acoustic black holes for the isolation of vibrations in plates

Deng Jie[1]
State Key Laboratory of Mechanical Transmission, College of Automotive Engineering Chongqing University, Chongqing 400044, PR China

Guasch Oriol[2]
GTM - Grup de recerca en Tecnologies Mèdia, La Salle, Universitat Ramon Llull C/ Quatre Camins 30, 08022 Barcelona, Catalonia, Spain

Zheng Ling[3,*]
State Key Laboratory of Mechanical Transmission, College of Automotive Engineering Chongqing University, Chongqing 400044, PR China

ABSTRACT
In many common situations concerning the vibroacoustics of built-up structures, a plate gets excited at a limited region where it is connected to further structural elements, like beams or other supporting elements. To avoid the transmission of vibrations to the plate one would typically resort to elastic junctions. However, that is not always feasible and, even if it was, they may not provide enough isolation. It is proposed herein to increase the latter by resorting to ring-shaped ABH configurations consisting in, at least, one annular strip with a power-law decaying profile in the radial direction. The ring-shaped ABH strip is used to surround the external excitation area and prevent the transmission of vibrations to the rest of the plate. Designs including radial stiffeners are also presented to avoid excessive structural weakening. The numerical simulations carried out using a Rayleigh-Ritz approach with a Gaussian expansion for the flexural displacement field, show that the ring-shaped ABH constitute an efficient way to enhance vibration isolation in plates.

Keywords: Acoustic black holes (ABH), Vibration isolation, Retarding waveguides, Ring-shaped ABH, Annular ABH
I-INCE Classification of Subject Number: 46

1. INTRODUCTION

The ABH effect in beams and plates can be achieved with a tailored wedge, or indentation, whose thickness *h* follows a power-law profile ($h=\varepsilon x^m$), which reaches a zero value at the tip (x=0), see [1]. Flexural waves traveling in the wedge will expend an infinite amount of time to reach the boundary, resulting in a zero reflection coefficient.

[1] dengjie@cqu.edu.cn
[2] oriol.guasch@salle.url.edu
[3,*] zling@cqu.edu.cn, corresponding author

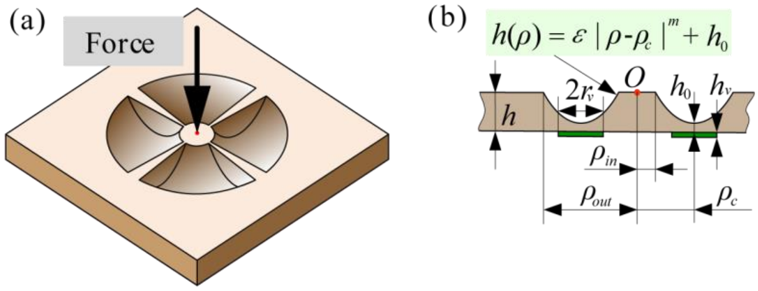

Figure 1 (a) 3D scheme of proposed annular ABH with harmonic force exerted at its center, (b) cross sectional view of the annular ABH plate, with viscoelastic layers located in the ABH center.

In practice, however, a truncation thickness will always exist due to manufacturing limitations, which would result in substantial wave reflection. To a good extent, this is usually remedied by placing viscoelastic layers [2], or passive constrained viscoelastic layers [3], at the wedge tip or indentation center, among other options [4,5].

To date, most ABH designs for plates consist in circular cuneate indentations [6,7,8,9], or rectangular ones with parabolic profiles [10,11]. Very recently, annular ABHs to reduce propagative Bloch-Floquet waves in periodically supported cylindrical shells have been also suggested [13]. It is to be mentioned that arrays of circular ABHs in plates have been shown to exhibit remarkable properties, which make them not only suitable for vibration suppression, but also for further applications such as energy harvesting [14], or wave manipulation [15].

In this work, we propose the design of ring-shaped ABHs, for vibration isolation in plates. In many built-up structures, plates are excited in a finite region, e.g., a beam-plate connection, and standard elastic junctions may not provide enough isolation. Ring-shaped ABHs could be used to surround the excitation area and dissipate its energy thanks to the ABH effect. Several configurations of ABHs have been tested, which include the insertion of stiffeners to avoid structural weakening, and the combination of several concentric ABHs to further reinforce isolation. The performance of the ABHs have been characterized through the Rayleigh-Ritz method, using Gaussian functions to expand the transverse displacement [3,9].

2. RING-SHAPED ABH MODELLING

2.1 ABH geometry

A 3D view of the proposed ring ABH structure for a plate is shown in Figure 1a, with the excitation point located at its center, where we establish the origin of coordinates O. The considered plate has dimensions $2a\times2a\times h$ and its geometric parameters are specified in Figure 1b. As observed, the inner radius is designated by ρ_{in} and the outer one by ρ_{out}. Hence, the width of the ring ABH is given by $2r_{abh}=\rho_{out}-\rho_{in}$, with the ABH center being at a radial distance $\rho_c=(\rho_{out}+\rho_{in})/2$. The radial power law profile for the ABH thickness is $h(\rho)=\varepsilon|\rho-\rho_c|^m+h_0$ ($m\geq2$). Moreover, an annular viscoelastic layer with uniform thickness h_v, width $2r_v$ and centerline radius ρ_c, is attached to the ABH to dissipate energy. Besides, note that instead of being a continuous ring, the ABH has been reinforced with some stiffeners to prevent structural weakness.

2.2 Admissible basis function

The ABH behavior has been investigated by means of a semi-analytical approach, in the framework of the Rayleigh-Ritz method. We consider the Love-Kirchhoff theory, which allows one to express the displacement field in the ABH plate as,

$$\begin{bmatrix} u & v & w \end{bmatrix}^{\mathrm{T}} = \begin{bmatrix} -z\dfrac{\partial w}{\partial x} & -z\dfrac{\partial w}{\partial y} & w(x,y,z) \end{bmatrix}^{\mathrm{T}}, \tag{1}$$

where w is the transverse displacement. We expand the latter by a set of basis functions

$$w(x,y,t) = \sum_i a_i(t)\varphi_i(x,y) = \mathbf{a}^{\mathrm{T}}\boldsymbol{\varphi} = \boldsymbol{\varphi}^{\mathrm{T}}\mathbf{a}, \tag{2}$$

with $\varphi_i(x,y)$ representing the i^{th} basis function and $a_i(t)$ its corresponding weight coefficient, which has to be determined. $\mathbf{a}$ and $\boldsymbol{\varphi}$ in Equation 2 are column vectors with entries $a_i(t)$ and $\varphi_i(x,y)$. With the help of the Kronecker product, $\boldsymbol{\varphi}$ can be expressed as the combination,

$$\boldsymbol{\varphi} = \boldsymbol{\alpha} \otimes \boldsymbol{\beta}, \tag{3}$$

where $\boldsymbol{\alpha}$ and $\boldsymbol{\beta}$ respectively represent column vectors,

$$\begin{aligned} \boldsymbol{\alpha} &= \left[\alpha_1(x), \alpha_2(x), ..., \alpha_i(x), ..., \alpha_m(x)\right]^{\mathrm{T}} \\ \boldsymbol{\beta} &= \left[\beta_1(y), \beta_2(y), ..., \beta_i(y), ..., \beta_n(y)\right]^{\mathrm{T}} \end{aligned}, \tag{4}$$

with $\alpha_i(x)$ being the i^{th} basis function in the x direction and $\beta_i(y)$ the i^{th} basis function in the y direction.

In this paper, Gaussian functions are chosen for $\alpha_i(x)$ and $\beta_i(y)$, following the developments in [3,9]. Analogous to what occurs when employing wavelet transforms (see e.g., [16,17]), one can build a set of Gaussian basis functions through dilations and translations. The elements in Equation 4 become

$$\alpha_{k_i}^{j}(x) = 2^{\frac{j}{2}} \exp\left[-\frac{\left(2^j x - k_i\right)^2}{2}\right], \quad \beta_{r_i}^{p}(y) = 2^{\frac{p}{2}} \exp\left[-\frac{\left(2^p y - r_i\right)^2}{2}\right]. \tag{5}$$

The indices j, p are scaling parameters that respectively squeeze or stretch the original function in the x and y directions. Similarly, k and r stand for translation parameters to move the functions in the x and y directions.

2.3 Equations of motion

The equations of motion for the plate with a ring ABH indentation can be obtained as follows. We start writing the Lagrangian operator from the kinetic and potential energies. The kinetic energy E_k is given by

$$E_k = \frac{1}{2}\int_{-b}^{b}\int_{-a}^{a} \rho h(x,y)\,\dot{w}^2 \mathrm{d}x\mathrm{d}y = \frac{1}{2}\int_{-b}^{b}\int_{-a}^{a} \rho h(x,y)\,\dot{\mathbf{a}}^{\mathrm{T}}\boldsymbol{\varphi}\boldsymbol{\varphi}^{\mathrm{T}}\dot{\mathbf{a}}\mathrm{d}x\mathrm{d}y \equiv \frac{1}{2}\dot{\mathbf{a}}^{\mathrm{T}}\mathbf{M}\dot{\mathbf{a}}, \tag{6}$$

where ρ denotes the density, and [-a, a] and [-b, b] the integration limits in the x and y directions. Likewise, the potential energy E_p can be expressed as

$$\begin{aligned}
E_p &= \frac{1}{2}\int_{-b}^{b}\int_{-a}^{a} D(x,y)\begin{bmatrix} \left(\frac{\partial^2 w}{\partial^2 x}\right)^2 + \left(\frac{\partial^2 w}{\partial^2 y}\right)^2 + v\left(\frac{\partial^2 w}{\partial x^2}\frac{\partial^2 w}{\partial y^2} + \frac{\partial^2 w}{\partial y^2}\frac{\partial^2 w}{\partial x^2}\right) \\ +2(1-v)\left(\frac{\partial^2 w}{\partial x \partial y}\right)^2 \end{bmatrix}\mathrm{d}x\mathrm{d}y \\
&= \frac{1}{2}\mathbf{a}^{\mathrm{T}}\left\{\int_{-b}^{b}\int_{-a}^{a} D(x,y)\begin{bmatrix} \frac{\partial^2 \boldsymbol{\varphi}}{\partial x^2}\frac{\partial^2 \boldsymbol{\varphi}^{\mathrm{T}}}{\partial x^2} + \frac{\partial^2 \boldsymbol{\varphi}}{\partial y^2}\frac{\partial^2 \boldsymbol{\varphi}^{\mathrm{T}}}{\partial y^2} \\ +v\left(\frac{\partial^2 \boldsymbol{\varphi}}{\partial x^2}\frac{\partial^2 \boldsymbol{\varphi}^{\mathrm{T}}}{\partial y^2} + \frac{\partial^2 \boldsymbol{\varphi}}{\partial y^2}\frac{\partial^2 \boldsymbol{\varphi}^{\mathrm{T}}}{\partial x^2}\right) \\ +2(1-v)\frac{\partial^2 \boldsymbol{\varphi}}{\partial x \partial y}\frac{\partial^2 \boldsymbol{\varphi}^{\mathrm{T}}}{\partial y \partial x} \end{bmatrix}\mathrm{d}x\mathrm{d}y\right\}\mathbf{a} \qquad (7) \\
&\equiv \frac{1}{2}\mathbf{a}^{\mathrm{T}}\mathbf{K}\mathbf{a},
\end{aligned}$$

with v standing for the Poisson ratio, $D(x, y)$ for the local flexural rigidity and $E^* = E(1+\mathrm{j}\eta)$ for the complex Young's modulus with material loss factor η.

On the other hand, the work done by the external force onto the system is

$$W = \int_{-b}^{b}\int_{-a}^{a} f(t)w(x,y,t)\mathrm{d}x\mathrm{d}y = f(t)\mathbf{a}^{\mathrm{T}}\int_{-b}^{b}\int_{-a}^{a}\boldsymbol{\varphi}\mathrm{d}x\mathrm{d}y = \mathbf{a}^{\mathrm{T}}\left[f(t)\int_{-b}^{b}\int_{-a}^{a}\boldsymbol{\varphi}\mathrm{d}x\mathrm{d}y\right] \equiv \mathbf{a}^{\mathrm{T}}\mathbf{f}(t). \quad (8)$$

From Equations 6 to 8, we can proceed as usual to construct the Lagrangian function,

$$L = E_k - E_p + W = \frac{1}{2}\dot{\mathbf{a}}^{\mathrm{T}}\mathbf{M}\dot{\mathbf{a}} - \frac{1}{2}\mathbf{a}^{\mathrm{T}}\mathbf{K}\mathbf{a} + \mathbf{a}^{\mathrm{T}}\mathbf{f}(t). \quad (9)$$

The Euler-Lagrange equations $\frac{\partial}{\partial t}\left(\frac{\partial L}{\partial \dot{\mathbf{a}}}\right) - \frac{\partial L}{\partial \mathbf{a}} = 0$ will then provide the linear matrix equations of motion,

$$\mathbf{M}\ddot{\mathbf{a}}(t) + \mathbf{K}\mathbf{a}(t) = \mathbf{f}(t). \quad (10)$$

Under harmonic regime, the force and response vectors can be written as

$$\mathbf{f}(t) = \hat{\mathbf{F}}e^{\mathrm{j}\omega t}, \ \ \mathbf{a}(t) = \hat{\mathbf{A}}e^{\mathrm{j}\omega t}, \quad (11)$$

where $\hat{\mathbf{F}}$ and $\hat{\mathbf{A}}$ respectively denote the amplitude vectors of the external force and the response. Substituting Equation 11 into Equation 10 yields

$$\left(\mathbf{K}-\omega^2\mathbf{M}\right)\hat{\mathbf{A}}=\hat{\mathbf{F}} \tag{12}$$

Equation 12 has been used to analyze the various ring-shaped ABH configurations. In practice, Equation 12 is first obtained for the bare plate and then, the matrix replacing strategy of [9] is applied to embed the ABHs in it.

3. NUMERICAL RESULTS

In this section, we present the performance of three different types of ring-shaped ABHs concerning vibration isolation. These are an ABH made of a ring containing small conventional circular ABHs, a continuous ring-shaped ABH and a stiffened ring-shaped ABH. Those will be respectively referred to as the *circle-ring* ABH, the *annular* ABH and the *stiffened-annular* ABH. Two main aspects will be examined: i) The effects of considering several concentric ABHs with identical width; ii) The effects of splitting a big annular ABH into smaller ones.

The geometrical and physical parameters of the ABHs used in the simulations to be presented in subsequent sections are given in Table 1.

Table 1 Material and geometrical parameters of the proposed ABH models

Material parameter	**Geometrical parameters**	
E_p=210 GPa	h=0.01 m	h_v=0.0025 m
ρ_p=7800 kg/m^3	ε=3.3879 1/m	r_v=0.0415 m
η_p= 0.005	a=b=0.5 m	
v_p= 0.3	h_0=0.0005 m	
E_v= 5 GPa	ρ_{in}=0.069 m	
ρ_v=7800 kg/m^3	ρ_{out}=0.175 m	
η_v= 0.5	ρ_c=0.122 m	

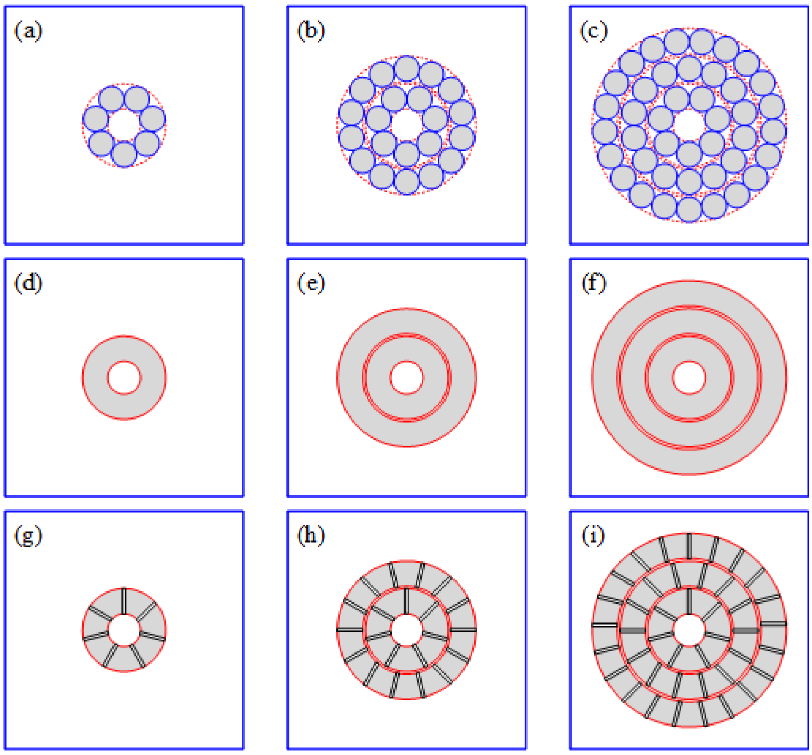

Figure 2 Geometries for the (a)-(c) The circle-ring ABHs, (d)-(f) annular ABHs, (g)-(i) rigid annular ABHs.

3.1 Increasing the number of concentric ABHs

The tested configurations in this section are illustrated in Figure 2. For each of them, we will compute the transmission loss (TL) between the vibration of the excitation area surrounded by the ABH (interior of the most inner red dashed circle in Figure 2), and the vibration of the receiver area (exterior of the most outer red dashed circle in Figure 2).

The TL is computed as the logarithmic quotient between the mean squared velocity at the excitation area and that of the receiver area, namely,

$$\mathrm{TL} = 10\log_{10}\frac{\left\langle v^2\right\rangle_{A_E}}{\left\langle v^2\right\rangle_{A_R}} \tag{13}$$

The first ABH is that of Figure 2a, which consists in a ring arrangement of seven conventional circular ABH indentations. For further isolation, in Figures 2b and 2c we consider the addition of outer concentric circle-ring ABHs. Figure 2b contains an additional layer with fourteen circle-ring ABHs, while a third layer is also included in Figure 2c, with twenty-one supplementary ABHs.

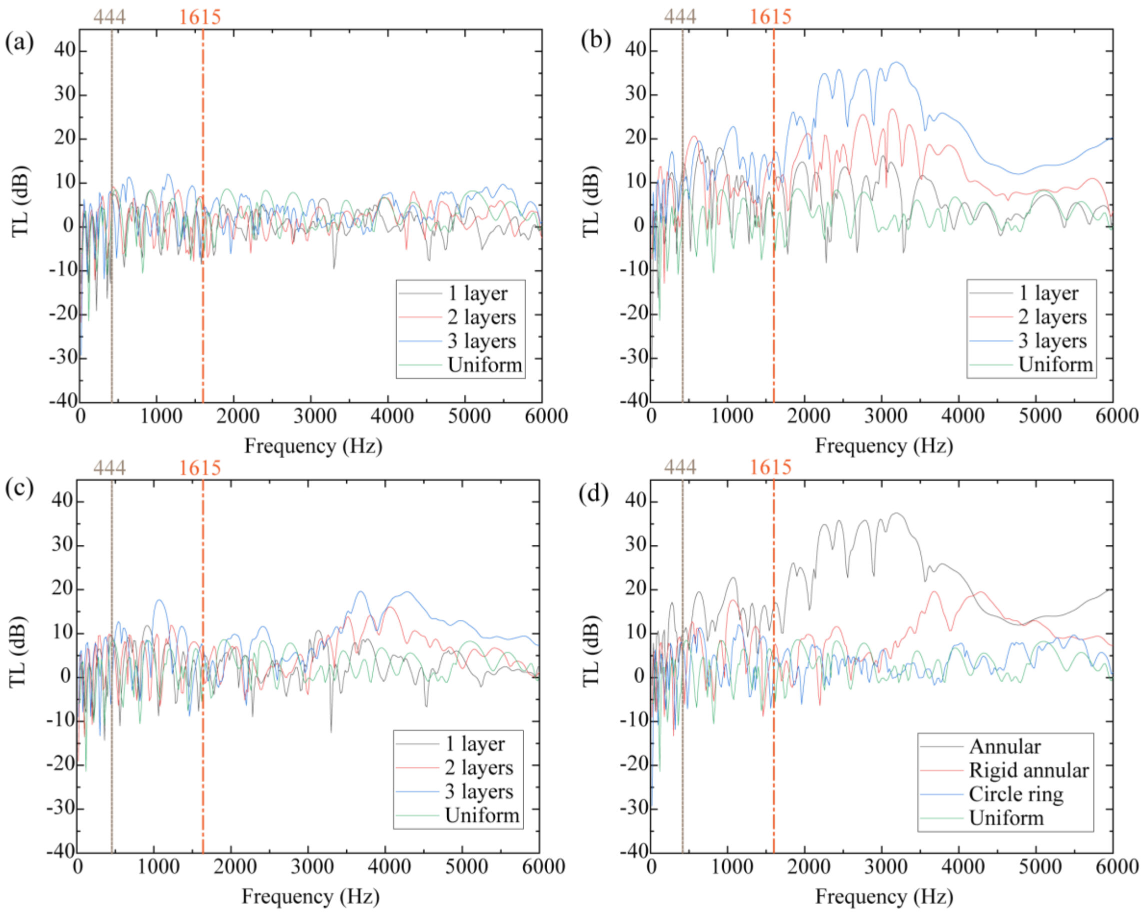

Figure 3 Transmission loss (TL) for (a) circle-ring ABHs, (b) annular ABHs, (c) stiffened-annular ABHs and (d) comparisons between ABHs for the three concentric ring cases. Vertical lines indicate the diameter and smoothness cut-on frequencies, f_r=444 Hz and f_ε=1615 Hz.

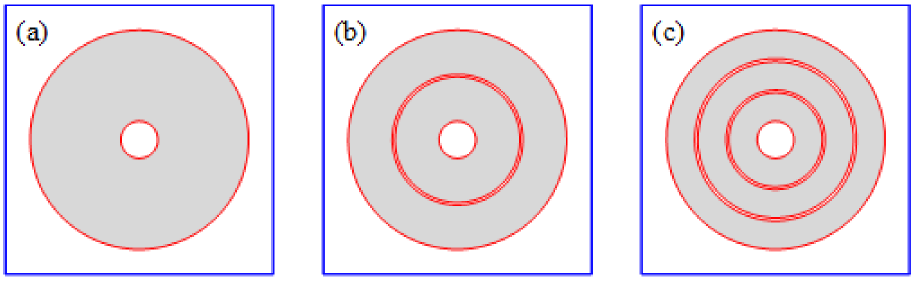

Figure 4 (a) One big annular ABH, splitting it into (b) 2 and (c) 3 smaller annular ABHs.

The second set of ABHs is shown in Figures 2d to 2f. Figure 2d presents an annular ABH, which is respectively complemented with one and two additional concentric ABHs in Figures 2e and 2f, analogously to what was done for the circle-ring ABH. Given that a continuous annular ABH may result in a substantial weakening of the structure, in Figure 2g we have included some stiffeners to the annular ABH. Figures 2h and 2i contain two and three concentric annular-stiffened ABHs. Note that to reinforce isolation, the stiffeners at the different concentric ABHs have been placed at different angular locations.

The TLs for the nine cases in Figure 2 are plotted in Figure 3, where we have also displayed the ABH diameter and smoothness cut-on frequencies as vertical lines. The ABHs effect takes place well beyond the second one. The results for the circle-ring ABHs are shown in Figure 3a, those of the annular ABHs in Figure 3b and those of the stiffened-annular ABHs in Figure 3c. As observed in all figures, the TL increases with the number of concentric ABHs, as one could expect. However, in the case of circle-ring ABHs (Figure 3a), the improvements are not significant if compared to the uniform plate, even when considering three concentric rings. As opposed, the annular ABHs perform remarkably well in mid to high frequencies (TL up to 35 dB between 2000Hz and 4000Hz, see Figure 3b). The stiffened-annular ABHs in Figure 3c also work well, but at somewhat higher frequencies and with less intensity (TL up to 20 dB between 3500 and 4500 Hz). For a clearer comparison, the TLs for the three concentric ABHs of Figures 2c, 2f and 2i are presented in Figure 3d. Clearly, the annular ABH is by far the best option, followed by the stiffened-annular ABH. The effect of the stiffeners is very noticeable, as seen in the figure. Besides, it is also apparent that the circle-ring ABH should be discarded because it only slightly improves the behavior of the uniform plate at some frequencies, while at others it even performs worse.

3.2 Effects of annular ABH dimensions

From the precedent discussion, it follows that the annular ABHs constitute the best option in terms of vibration isolation. Therefore, we will next focus on them and complement the previous results considering a case in which we have a fixed annular surface where to place the ABH. The situation is illustrated in Figure 4. Figure 4a contains a single, large, ABH which becomes split in two ABHs in Figure 4b, and in three ABHs in Figure 4c. Note that the configuration of Figure 4c coincides with that of Figure 2f. Besides, observe that the splitting procedure will result in ABHs of steeper profile, thus augmenting the cut-on smoothness frequency (see e.g. [8,9]). Those are respectively given by 157 Hz, 630 Hz and 1615 Hz for the ABHs in Figures 4a, 4b and 4c.

As illustrated in Figure 5, the TL of the single annular ABH becomes stable (few oscillations) once surpassed about three times its smoothness frequency. The TLs for the 2 and 3 ABHs show an analogous behavior. This means that for a fixed ABH area, increasing the number of ABHs does not result in a big difference beyond the highest cut-on smoothness frequency. However, the performances of the three ABHs are very different below the cut-on frequencies. The reason for that is a combination of the ABH effect together with the changes in the plate's rigidity, due to the ABH indentations. The steeper ABHs tend to increase the reflection the out-going waves from the excitation area, augmenting its vibration level, and therefore the TL values at low frequencies. The TLs can be considerably large: up to 35 dB between 2000 and 4000 Hz for the three ABH configuration (as already observed in Figures 2b and 2d), and up to 25 dB between 500 and 1200 Hz for the two ABH arrangement.

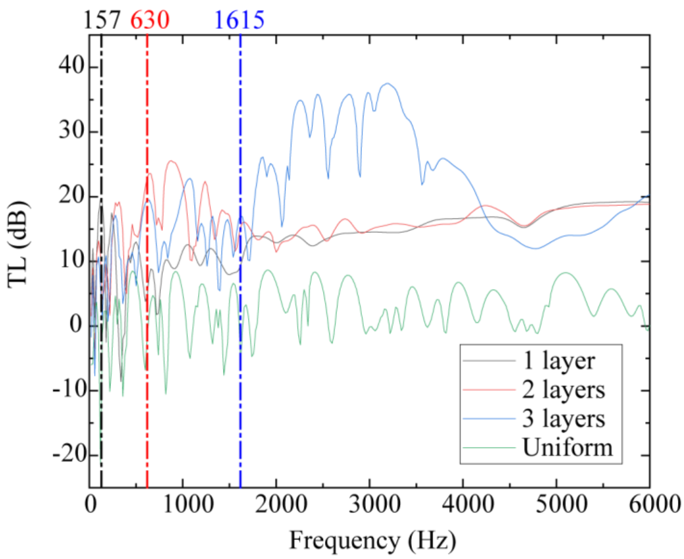

Figure 5 Transmission losses (TL) when splitting 1 big annular ABH (f_ε=157 Hz) into 2 (f_ε=630Hz) and 3 (f_ε=1615 Hz) ABHs.

4. CONCLUSIONS

This paper suggests the design of ring-shaped ABHs surrounding an excitation area on a plate for vibration isolation. Three different types of ABHs have been simulated consisting of ring distributions of circular ABHs, annular ABHs and stiffened annular ABHs. The simulations have been carried out by means of a semi-analytical method that uses Gaussian basis functions to decompose the ABH plate displacement field, under the framework of the Rayleigh-Ritz method. The performance of the ABHs has been characterized computing the transmission loss (TL) between the vibration at the plate excitation area and that at the plate receiver area, aft the ABH.

Two critical aspects have been tested: the effect of increasing the number of concentric ABHs and that of splitting a big annular ABH into smaller ones. The former shows the inclusion of more ABHs helps increasing the TL, as expected. Annular ABHs exhibit the best behavior. The inclusion of stiffeners on them, however, significantly alter their performance, so they should be carefully designed. Finally, the circle-ring ABHs can be discarded because they show a similar behavior to that of a uniform plate. In what concerns splitting an annular ABH into several ones, the results show that this has no effect beyond the cut-on smoothness frequency of the smaller ABH, while substantial differences can be appreciated below that. Those are partially attributed to the ABH effect and partially to back reflections to the excitation area, when increasing the slope of the ABH profiles.

5. ACKNOWLEDGEMENTS

This work has been completed while the first author was performing a two-year PhD stay at La Salle, Universitat Ramon Llull, funded by the National Natural Science

Foundation of China under Grant (51875061) and the China Scholarship Council (CSC No. 201806050075). The authors gratefully acknowledge this support as well as the in-kind assistance from La Salle, Universitat Ramon Llull, and the Chongquing University to make that collaboration possible. The second author would also like to thank l'Obra Social de la Caixa and the Universitat Ramon Llull for their support under grant 2018-URL-IR2nQ-031

6. REFERENCES

1. M.A. Mironov, *Propagation of a flexural wave in a plate whose thickness decreases smoothly to zero in a finite interval*, Soviet Physics Acoustics, (1988);34:318-319
2. V.V. Krylov and F.J.B.S. Tilman, *Acoustic 'black holes' for flexural waves as effective vibration dampers*, J. Sound Vib., (2004);274:605-619.
3. J. Deng, L. Zheng, P. Zeng, Y. Zuo and O. Guasch, *Passive constrained viscoelastic layers to improve the efficiency of truncated acoustic black holes in beams,* Mech. Sys. Signal Process., (2019);118:461-476.
4. L. Tang and L. Cheng, *Enhanced Acoustic Black Hole effect in beams with a modified thickness profile and extended platform*', J. Sound Vib., (2017);391:116-126.
5. V. Denis, A. Pelat, C. Touzé and F. Gautier, *Improvement of the acoustic black hole effect by using energy transfer due to geometric nonlinearity*, Int. J. Non Linear Mech., (2017);94:134-145.
6. D. O'Boy and V. Krylov, *Damping of flexural vibrations in circular plates with tapered central holes*, J. Sound Vib., (2011);330(10):2220–2236.
7. E. Bowyer, D.O'Boy, V. Krylov and F. Gautier, *Experimental investigation of damping flexural vibrations in plates containing tapered indentations of power-law profile*, Appl. Acoust., (2013);74 (4):553–560.
8. S. Conlon, J. Fahnline and F. Semperlotti, *Numerical analysis of the vibroacoustic properties of plates with embedded grids of acoustic black holes*, J. Acoust. Soc. Am., (2015);137(1):447–457.
9. J. Deng, L. Zheng, O. Guasch, H. Wu, P. Zeng and Y. Zuo, *Gaussian expansion for the vibration analysis of plates with multiple acoustic black holes indentations, Submitted* (2019).
10. D. O'Boy and V. Krylov, *Vibration of a rectangular plate with a central power-law profiled groove by the Rayleigh-Ritz method*, Appl. Acoust., (2016);104:24-32.
11. L. Ma, S. Zhang and L. Cheng, *A 2D Daubechies wavelet model on the vibration of rectangular plates containing strip indentations with a parabolic thickness profile*, J. Sound Vib., (2018);429:130-146.
12. Z. Liuxian, C. C. Stephen and S. Fabio, "*Broadband energy harvesting using acoustic black hole structural tailoring*", Smart Materials and Structures (2014)
H. Zhu and F. Semperlotti, "*Phononic thin plates with embedded acoustic black holes*", Physical Review B (2015).
13. J. Deng, O. Guasch, L. Maxit and L. Zheng, *Annular acoustic black holes to reduce propagative Bloch-Floquet flexural waves in periodically supported cylindrical shells, Inter-Noise 2019, 16-19 June, Madrid, Spain. Submitted* (2019).
14. L. Zhao, S. Conlon, F. Semperlotti, *Broadband energy harvesting using acoustic black hole structural tailoring*, Smart Mater. Struct. (2014);23:065021.
15. H. Zhu and F. Semperlotti, *Two-dimensional structure-embedded acoustic lenses based on periodic acoustic black holes,* J. Appl. Phys., (2017);122:065104.

16. L. Tang, L. Cheng, H. Ji and J. Qiu, *Characterization of acoustic black hole effect using a one-dimensional fully-coupled and wavelet-decomposed semi-analytical model*, J. Sound Vib., (2016);374:172-184.
17. L. Ma, S. Zhang and L. Cheng, *A 2D Daubechies wavelet model on the vibration of rectangular plates containing strip indentations with a parabolic thickness profile*, J. Sound Vib. (2018):429:130-146.